Received: 19 April 2023 | Revised: 29 June 2023 | Accepted: 18 July 2023

DOI: 10.1111/cts.13604

ARTICLE

TXNDC12 knockdown promotes ferroptosis by modulating SLC7A11 expression in glioma

Hao Yu | **Kai Zhu** | **Minjie Wang** | **Xiaobing Jiang**

Department of Neurosurgery, Union Hospital, Tongji Medical College, Huazhong University of Science and Technology, Wuhan, China

Correspondence
Minjie Wang and Xiaobing Jiang, Department of Neurosurgery, Union Hospital, Tongji Medical College, Huazhong University of Science and Technology, Wuhan 430021, China.
Email: 752796545@qq.com and my229836179@163.com

Abstract

Ferroptosis is an iron-dependent cell death process mainly triggered by reactive oxygen species (ROS) and lipid peroxidation. Thioredoxin domain protein 12 (TXNDC12) promotes the development of some tumors; however, its function in tumor ferroptosis remains unclear. In this study, we found that knockdown of TXNDC12 promoted erastin-induced increase in ROS, lipid peroxidation, and Fe^{2+} levels, and decreased glutathione content. TXNDC12 is involved in ferroptosis by regulating SLC7A11. Further studies showed that TXNDC12 knockdown promoted an erastin-induced decrease in glioma cell viability. Overall, TXNDC12 played a significant role in ferroptosis by modulating SLC7A11 expression. Thus, TXNDC12 and ferroptosis may provide new targets for the treatment of gliomas.

Study highlights

WHAT IS THE CURRENT KNOWLEDGE ON THE TOPIC?

Several genes are involved in the regulation of iron levels. Tumor cells rely on their strong antioxidant capacity to escape ferroptosis. Therefore, the study of ferroptosis may be an important research direction for interfering with tumor proliferation and invasion.

WHAT QUESTION DID THIS STUDY ADDRESS?

We investigated the role and regulatory mechanisms of TXNDC12 in ferroptosis in gliomas, and whether TXNDC12 might be a promising target for future glioma treatment.

WHAT DOES THIS STUDY ADD TO OUR KNOWLEDGE?

TXNDC12 knockdown promoted erastin-induced increase in reactive oxygen species, lipid peroxidation, and Fe^{2+} levels and decreased glutathione content. TXNDC12 is involved in ferroptosis by regulating SLC7A11. Further studies showed that TXNDC12 knockdown promoted erastin-induced decrease in glioma cell viability.

Hao Yu and Kai Zhu contributed equally to this work and share first authorship.

HOW MIGHT THIS CHANGE CLINICAL PHARMACOLOGY OR TRANSLATIONAL SCIENCE?

TXNDC12 is involved in ferroptosis, which may be a direction for future studies on ferroptosis in glioma. The study of TXNDC12 inhibitors may provide a new direction for the treatment of gliomas.

INTRODUCTION

Gliomas are the most common malignant tumors of the central nervous system. Owing to their diffuse invasion, complete surgical resection is unrealistic because even if surgical resection is satisfactory, most patients experience recurrence.[1] Diffuse gliomas are characterized by substantial heterogeneity in tumor biology and clinical behavior.[2] Generally, gliomas spread rapidly to other brain regions; however, distant metastasis rarely occurs because the blood–brain barrier (BBB) limits extra-brain metastasis.[3] Another characteristic of diffuse gliomas is their ability to undergo malignant transformation. Low-grade gliomas inevitably recur and evolve to a higher grade (World Health Organization [WHO] III-IV) over time.[4] Although temozolomide (TMZ) is the main chemotherapeutic drug used for glioma treatment, resistance to TMZ has become an inevitable obstacle to glioma chemotherapy, often leading to poor prognosis and treatment failure.[5] However, in the absence of TMZ treatment, the survival rate decreases. Therefore, to improve survival rates, it is necessary to develop novel targeted treatment strategies.[6]

In iron-dependent cell death, ferroptosis mainly manifests in response to reactive oxygen species (ROS) and lipid peroxidation, the accumulation of which leads to cell death.[7,8] System Xc^- is a cystine transporter on the surface of cell membranes and is composed of the light-chain subunit solute carrier family 7 member 11 (SLC7A11) and heavy-chain subunit solute carrier family 3 member 2 (SLC3A2).[9] SLC7A11 plays an important role in the exchange of intracellular glutamate and extracellular cystine in equal proportions. After entering the intracellular environment, cystine is reduced to cysteine, which is used in the synthesis of glutathione (GSH).[10] Notably, GSH is critical ferroptosis inhibition.[11] SLC7A11 is highly expressed in some cancers, and overexpression of SLC7A11 promotes tumor growth by inhibiting ferroptosis.[12] With increasing research on ferroptosis, its regulatory mechanism in tumors has become increasingly clear, and accumulating evidence suggests that promoting ferroptosis in tumors is a promising tumor treatment strategy.[13]

Thioredoxin domain protein 12 (TXNDC12), also known as ERp19, ERp18, and hTLP19, belongs to the thioredoxin superfamily. It plays a critical role in defense against endoplasmic reticulum stress and is involved in the occurrence and progression of some tumors.[14,15] TXNDC12 is upregulated in hepatocellular carcinoma and promotes epithelial-mesenchymal transformation (EMT) and metastasis of hepatocellular carcinoma by activating catenin.[15] TXNDC12 is highly expressed in cervical cancer cell lines and tissues and higher levels of expression are associated with a poor prognosis. TXNDC12 promotes the migration of cervical cancer cells and formation of endothelial cells.[16] In gastric cancer, TXNDC12 promotes tumor growth, migration, and invasion.[17] In contrast, low TXNDC12 expression is associated with poor prognosis in patients with lung adenocarcinoma.[18] In summary, TXNDC12 is associated with the occurrence and progression of some tumors. Wang et al.[19] examined The Cancer Genome Atlas (TCGA) database and showed that high expression of TXNDC12 is associated with poor prognosis of glioma. However, the specific role of TXNDC12 in glioma remains unclear.

Here, we found that TXNDC12 was downregulated in glioma cells following erastin treatment. Using Gene Set Enrichment Analysis (GSEA), we concluded that TXNDC12 is involved in GSH metabolism, a key process in ferroptosis. TXNDC12 regulated erastin-induced ferroptosis in glioma cells by directly binding to SLC7A11. Our study on the role and regulation of TXNDC12 in glioma ferroptosis suggests that TXNDC12 is a promising target for glioma treatment.

MATERIALS AND METHODS

Data sources and clinical samples

The human glioma survival data were extracted from TCGA (https://cancergenome.nih.gov/).[20] Tissue samples obtained from 24 patients with glioma and 10 patients with paracancer were acquired from Wuhan Union Hospital, Tongji Medical College, Huazhong University of Science and Technology, Wuhan, China (Tables S2 and S4). The participants signed informed consent forms before their samples and data were used in the study. This study followed the principles of the Declaration of Helsinki and was approved by the Ethics Committee of Tongji Medical College, Huazhong University of Science and Technology (protocol code: [2019] IEC (s742). Approval date: March 4, 2019).

Immunohistochemistry

Tissue sections were incubated with anti-TXNDC12 antibodies at 4°C and washed three times. The cells were then incubated with the secondary antibody for 30 min.[21] Sections of tissue were scored as follows: 0, 0%; (1) 1%–10%; (2) 11%–25%; (3) 26%–50%; (4) 51%–70%; and (5) 71%–100%. Staining intensity scoring: 0, negative; 1, weak staining; 2, moderate staining; and 3, strong staining. Based on the staining intensity and percentage of positive cells, the staining score was calculated, resulting in negative and positive groups.

Cell culture

Human glioma cell lines U251, U373, U87, LN18, A172, and LN229, and human glial cells were grown in Dulbecco's Modified Eagle Medium (DMEM) containing 10% fetal bovine serum and 100 mg/mL penicillin/streptomycin, respectively, and incubated at 37°C in 5% CO_2.

Western blot

Protein concentration was measured using bicinchoninic acid. The isolated proteins were separated by SDS-PAGE and incubated with anti-TXNDC12 antibodies after being transferred to a polyvinylidene fluoride membrane and blocked with 5% bovine serum albumin. Blots were washed, incubated for an hour with rabbit secondary antibodies at 25°C, and detected for 20 s with electrochemiluminescence reagents.[22]

Real-time quantitative reverse transcriptase-polymerase chain reactions

RNA was isolated from the tissue samples using Trizol reagent (Thermo Fisher Scientific). The SYBR Green real-time polymerase chain reaction (PCR) kit was used to perform real-time quantitative PCRs (RT-qPCRs), with glyceraldehyde 3-phosphate dehydrogenase as an internal control. Primer sequences are provided in Table S3. All RT-qPCR reactions were performed independently in triplicate.

Lentivirus production and transfection

Culture dishes with 90% density of 293T cells were prepared, and the culture medium was replaced with DMEM without penicillin and streptomycin. Opti-MEM, packaging plasmid, envelope plasmid, and transfection reagent HG were added to the 293T cells after transient mixing. After 72 h, the supernatant was collected, filtered, and stored at −80°C. Glioma cell lines were planted in 35 mm culture dishes at a cell density of ~30%–50%, and virus and transfection reagents were added.

Immunofluorescence

Paraformaldehyde and methanol were used to fix the cells, which were then blocked with 15% donkey serum for 1 h. The cells were then incubated with TXNDC12 rabbit antibody and SLC7A11 mouse antibody (Abcam, UK, 1:400 dilution) for 16 h at 4°C, and then incubated with Alexa 594 and 488 fluorescent secondary antibodies, respectively, in the dark, counterstained with 4′,6-diamidino-2-phenylindole, and observed and captured under a confocal laser scanning fluorescence microscope.

Functional enrichment analysis

The expression data relating to TXNDC12 were extracted from each sample in TCGA database and divided into high and low expression groups according to the median expression. The functional enrichment of the different expression was then analyzed with the Kyoto Encyclopedia of Genes and Genomes using the R software package "ggpolt2," with | log2fc | greater than 1 and a p value < 0.05 as the standard.

Colony formation assay

To assess the effects of erastin (HY-15763, MCE) on glioma cell lines, glioma cells were cultured in 60 mm dishes at a density of ~70% and treated with 10 μM erastin or DMSO for 24 h. The cells were digested and inoculated into a 6-well plate at 1000 cells/well. The cells were cultured for 14 days. Then the cells were fixed and stained with crystal violet dye for 1 h, washed, observed, and photographed under a microscope.

Glutathione assay

To explore the effect of ferroptosis inducers and inhibitors on the relative GSH content of glioma cells, the cells were analyzed using a total GSH assay kit (S0052; Beyotime). The cells were treated with a ferroptosis inducer (erastin) or ferroptosis inhibitor (ferr-1). Cells

were cultured in 50 mm dishes for 24 h with DMSO, 10 μM erastin, or 5 μM ferr-1. The cells were digested and subjected to the manufacturer's protocol for GSH measurement using a kinetic assay and the absorbance was read at 412 nm.

Malondialdehyde assay

The relative levels of lipid oxidation in the cells were detected using a lipid peroxidation malondialdehyde (MDA) assay kit (S0131m; Beyotime). DMSO, 10 μM erastin, or 5 μM ferr-1 were added to the cells for 24 h and tested according to the manufacturer's protocol. The MDA and thiobarbituric acid reaction resulted in a chromogenic reaction with a red colored product. MDA content in the cell lysates was determined using a microplate reader at 532 nm.

Iron assay

An iron assay kit (ab83366; Abcam) was used to measure the level of ferrous iron in the cells according to the manufacturer's instructions. The cells were treated with DMSO, 10 μM erastin, or 5 μM ferr-1 for 24 h, and a ferric reducing agent was added. After incubation for 30 min, an iron probe was added, and the cells were incubated in the dark for 1 h, and the absorbance was measured at 593 nm.

Cell viability assay

Cell viability was assessed using CCK-8 (bs350b; Biosharp). After seeding glioma cells in 96-well plates at 8000 cells/well, different doses of erastin (0, 3, 5, 10, 15, and 20 μM) were added, and the plates were incubated for 24 h. CCK-8 solution (10 μL) was added to each well, along with 100 μL of the medium. After 10 h of incubation at 37°C, the absorbance was measured at 450 nm using a microplate reader.

Lipid ROS measurement

To explore the effect of ferroptosis inducers and inhibitors on the relative levels of lipid ROS in glioma cells, the cells were analyzed by flow cytometry. We treated the cells with a ferroptosis inducer (erastin) or ferr-1. Cells were cultured in 50 mm dishes for 24 h in DMSO, 10 μM erastin, or 5 μM ferr-1. We used H2DCFDA (permeation probe H2DCFDA [DCFH-DA]) to detect ROS levels in cells. The cells were incubated with DMSO or 5 μM H2DCFDA solution at 37°C for 30 min, collected, suspended in fresh medium, and immediately analyzed by flow cytometry.

Co-immunoprecipitation and silver staining

To investigate whether TXNDC12 interacted with SLC7A11, we used protein A/G magnetic beads (HY-K0202, MCE) for co-immunoprecipitation studies. After washing the magnetic beads, the antibody (40 μg/mL) was incubated with the magnetic beads (4°C, 2 h) before washing away the unbound antibody. U251 cells were digested and lysed and the lysates were incubated with magnetic beads (4°C, 2 h). The beads were then washed three times.

After electrophoresis, the gel was placed in ~100 mL of fixing solution and vortexed at 25°C on a shaker for 20 min at 60–70 rpm. The fixing solution was removed, 100 mL of 30% ethanol was added, and the gel was vortexed at 25°C on a shaking table for 10 min at 60–70 rpm. Ethanol was poured off, and 100 mL of silver sensitizing solution was added. After washing, the silver solution was added, followed by vortexing for 10 min. The silver dye color development solution was added after washing, and when ideal bands appeared, the silver dye termination solution was added.

GST-pull down assay

GST or GST-SLC7A11 fusion proteins were purified using GSH sepharose beads. Glioma cell lines transfected with TXNDC12 were lysed, and the purified GST or GST fusion proteins were added to the extracted proteins, incubated at 4°C, and rotated overnight. Proteins were eluted and subjected to Western blot analysis.

Animal experiments

BALB/c female immunodeficient nude mice aged 4–5 weeks were acquired from Wuhan Shulaibao Biology and placed in a specific pathogen-free environment. To investigate the function of TXNDC12 in erastin-mediated antitumor activity in vivo, we used BALB/c female immunodeficient nude mice to construct a xenograft mouse model. Control, TXNDC12 knockdown (KD), or SLC7A11 U87 cells were transplanted into the craniums of BALB/c female immunodeficient nude mice (5×10^5 cells per mouse). Starting on day 7, erastin (15 mg/kg, intracranial injection twice every other day) was administered to treat the tumors in situ. After growing the nude mice for 3–4 weeks, imaging of small animals was performed

to observe the occurrence of intracranial tumors in the mice. The xenograft mouse model experiment was conducted according to procedures approved by the Animal Ethics Committee of Huazhong University of Science and Technology.

Statistical analysis

Analysis and mapping of the data were conducted using GraphPad Prism 8.3.0 and R software (R 4.0.3). The *p* values were calculated using two-tailed unpaired Student's *t*-tests and log rank tests with R software or GraphPad Prism 8.3.0. *, $p < 0.05$; **, $p < 0.01$; ***, $p < 0.001$; ****, and $p < 0.0001$. All in vitro experiments were performed with at least three biological replicates.

RESULTS

TXNDC12 is highly expressed in gliomas and is associated with poor prognosis

To explore the potential function of TXNDC12 in gliomas, we evaluated TXNDC12 expression in gliomas and adjacent normal tissues. An increase in TXNDC12 expression was observed in gliomas compared to that in normal adjacent normal tissues (Figure 1a,b). Tests using qPCR and immunohistochemistry (Figure 1c,d) showed that TXNDC12 expression levels were positively correlated with the glioma grade. As the glioma progressed from stage I to stage IV, the expression of ApoC1 increased. In addition, TXNDC12 expression levels were negatively correlated with the overall survival (OS) rate of patients with glioma, and the level of TXNDC12 was linked to a low survival rate of patients with gliomas (Figure 1e). The survival data of patients with glioma in TCGA database are shown in Table S1. Furthermore, the mRNA levels of TXNDC12 in TCGA and GTEx databases were analyzed online using GEPIA. We observed that low-grade glioma and glioblastoma tissues had higher levels of TXNDC12 mRNA than the normal tissues. Similar results were observed in urothelial bladder, esophageal, and liver hepatocellular carcinomas and colon, pancreatic, rectal, and stomach adenocarcinomas (Figure S1A).

TXNDC12 knockdown promoted ferroptosis in glioma cells

Knowledge of the signaling pathways of genes active in tumors may contribute to the treatment of tumor-related gene modifications. The poor prognosis of patients with high TXNDC12 expression may be related to the activation of certain signaling pathways in gliomas. To explore the role of TXNDC12 in glioma, GSEA was conducted in TCGA database to analyze the biological pathways that might be affected by differentially expressed TXNDC12. A significant difference was observed in the richness of the MSigDB dataset (kegg.v7.2. symbols.gmt; standardized $p < 0.05$). This indicates that the differential expression of TXNDC12 involves many biological pathways. We found that TXNDC12 expression was significantly correlated with the GSH metabolism pathway. Therefore, we hypothesized that TXNDC12 is involved in GSH metabolism, an important process in ferroptosis (Figure S1B). Co-expression analysis revealed that TXNDC12 was associated with the expression of ferroptosis-related genes (Figure S1C). Thus, TXNDC12 may be related to ferroptosis and may be involved in some ferroptosis processes. Erastin was added to U87 and U251 cells, and TXNDC12 mRNA levels were detected at 20 and 30 min and at 1, 2, 4, 8, 12, and 24 h after administration. We found that the mRNA levels of TXNDC12 gradually decreased with increasing administration time (Figure 2a,b). The protein level of TXNDC12 was detected at 0, 10, 20, and 30 min and at 1, 2, 4, and 8 h after administration, and gradually decreased (Figure 2c,d).

We constructed glioma cell lines, U87 and U251, and transfected them with empty vector, TXNDC12 KD or TXNDC12 overexpression plasmids to further investigate the relationship between TXNDC12 and ferroptosis. The qPCR and Western blot analysis showed that TXNDC12 KD and TXNDC12 overexpression effectively altered the expression of TXNDC12 (Figure S2A–D).

In the presence or absence of TXNDC12 KD, U87 and U251 cells were treated with ferr-1. During ferroptosis, lipid peroxidation reaction produces a large amount of lipid peroxidation products, which then gradually decompose during the oxidation reaction into a series of complex aldehydes, including MDA. The lipid peroxidation index was determined by measuring MDA levels. We found that the lipid peroxidation levels of U87 and U251 cells increased after TXNDC12 KD and that these increased levels could be inhibited by ferr-1 (Figure S3A). GSH is an important antioxidant that removes lipid peroxides from cells and prevents ferroptosis. TXNDC12 KD lowered GSH levels in U87 and U251 cells and these lowered GSH levels could be increased by ferr-1 (Figure S3B). A dynamic iron pool exists within the cells of the human body that maintains intracellular iron homeostasis. However, under various pathological conditions, excessive iron entering the cell leads to an overload of this pool. Fe^{2+} can undergo a Fenton reaction with hydrogen peroxide in the body, which can produce numerous hydroxyl radicals that peroxidate polyunsaturated fatty acids on the surface of biological plasma membranes, leading to a

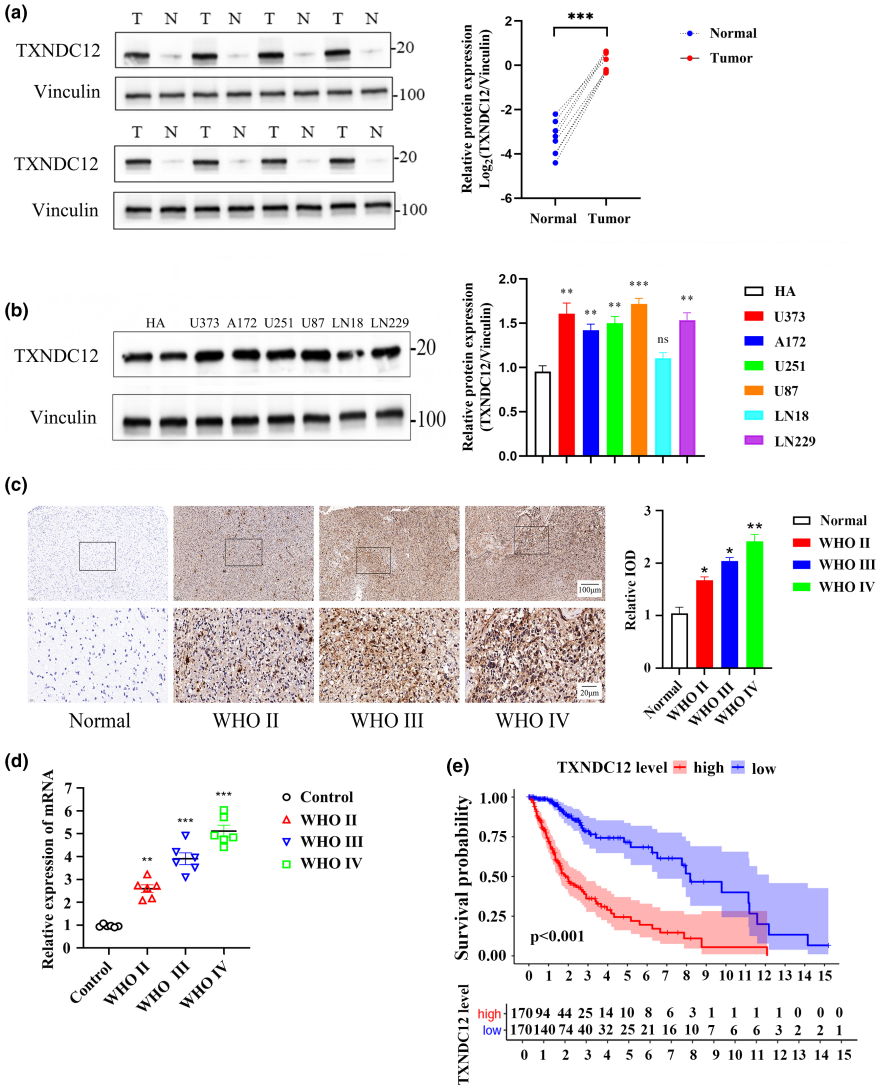

FIGURE 1 TXNDC12 is associated with poor prognosis in gliomas. (a) TXNDC12 expression determined by western blotting in glioma and paracancerous tissues. N: normal; T: tumor. (b) Relative protein expression of TXNDC12 in normal human astrocyte and glioma cell lines (U373, A172, U251, U87, LN18, and LN229), obtained by Western blotting. (c) Expression of TXNDC12 in adjacent normal tissues and gliomas of different grades, obtained by immunohistochemistry. (d) Expression of TXNDC12 in adjacent normal tissues and gliomas of different grades obtained using qPCR. (e) Overall survival curves of patients with high or low TXNDC12 expression from TCGA dataset. Data shown represent mean ± SD from three independent experiments. *$p < 0.05$; **$p < 0.01$; ***$p < 0.001$. ns, not significant; qPCR, quantitative polymerase chain reaction; TCGA, The Cancer Genome Atlas; WHO, World Health Organization.

large accumulation of lipid peroxides, cell membrane lysis, and ferroptosis. After TXNDC12 KD, Fe^{2+} and ROS levels increased in glioma cells, and these increased levels of Fe^{2+} and ROS were inhibited by ferr-1 (Figure S3C,D). This suggests that TXNDC12 KD can promote ferroptosis in glioma cells, and that this effect can be inhibited by ferr-1.

TXNDC12 knockdown promotes erastin-induced ferroptosis

The effect of erastin on ferroptosis in glioma cells was investigated using different doses of erastin (0, 3, 5, 10, 15, and 20 μM). We found that 5, 10, 15, and 20 μM erastin effectively reduced the survival rate of cells (Figure 2f). In addition, in the presence or absence of TXNDC12 KD, different concentrations of erastin were added to glioma cells to further study how TXNDC12 affects erastin-induced ferroptosis. Treatment with different concentrations of erastin significantly reduced the viability of cells in the TXNDC12 KD group compared with that in the control group (Figure 2f). We concluded that TXNDC12 KD significantly increased the decline in cell viability caused by erastin. The relative concentrations of MDA, GSH, Fe^{2+}, and ROS in glioma cells after erastin treatment were determined. TXNDC12 KD significantly promoted the

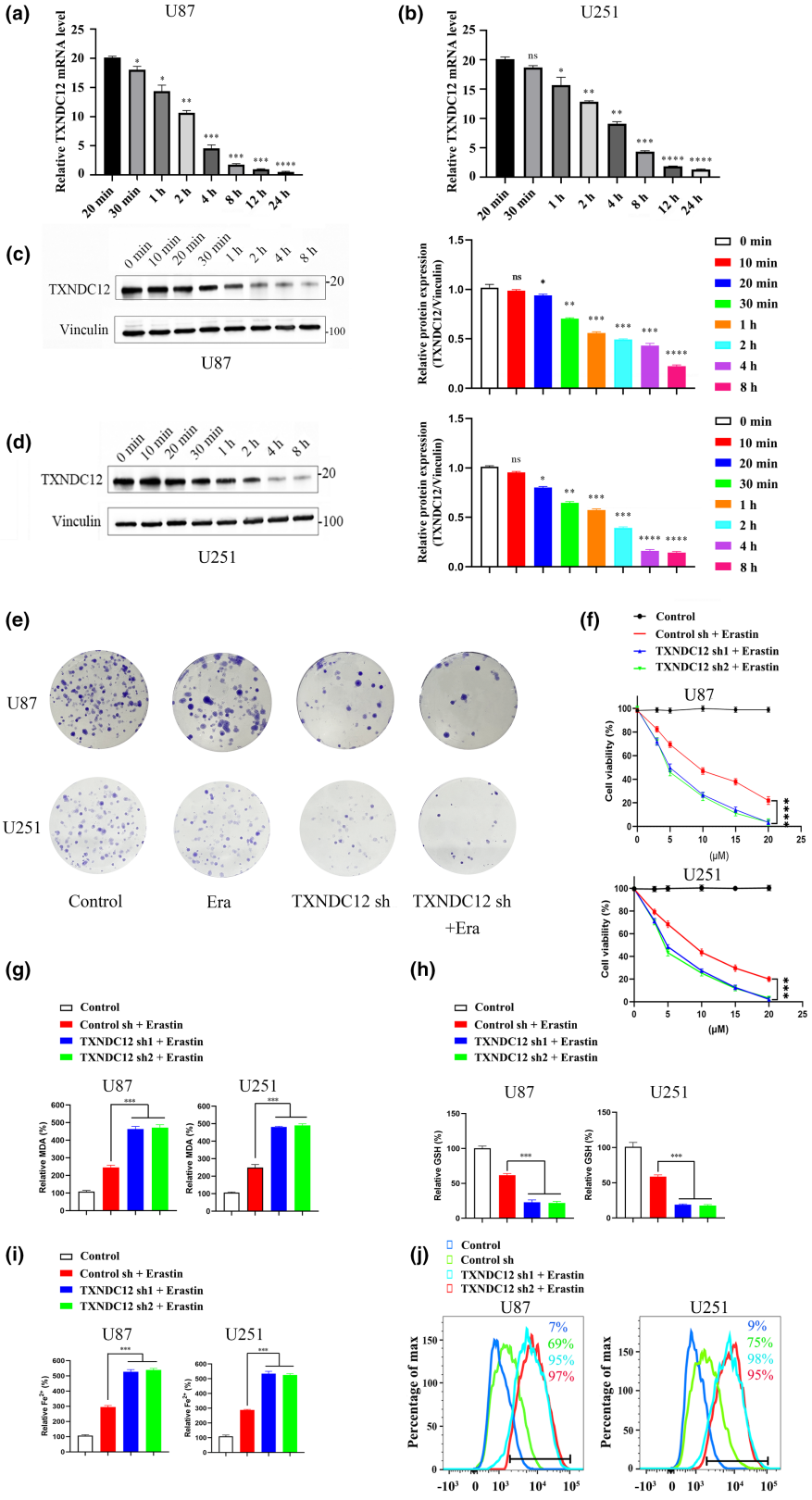

FIGURE 2 TXNDC12 knockdown promotes erastin-induced ferroptosis. (a) TXNDC12 mRNA levels were detected in U87 cells treated with 10 μM erastin for 20 and 30 min and 1, 2, 4, 8, 12, and 24 h. (b) TXNDC12 mRNA levels were detected in U251 cells treated with 10 μM erastin for 20 and 30 min and 1, 2, 4, 8, 12, and 24 h. (c) TXNDC12 protein levels in U87 cells treated with 10 μM erastin were detected by Western blotting at 0, 10, 20, and 30 min and at 1, 2, 4, and 8 h. (d) TXNDC12 protein levels in U251 cells treated with 10 μM erastin were detected by Western blotting at 0, 10, 20, and 30 min and at 1, 2, 4, and 8 h. (e) Representative images of the clonability analysis of U87 and U251 cells transfected with control sh or TXNDC12 KD and treated with DMSO or erastin (10 μM). (f) In the presence or absence of TXNDC12 knockdown, U87 and U251 cells were treated with erastin concentrations of 0, 3, 5, 10, 15, and 20 μM for 12 h to detect cell activity. Cells transfected with the indicated constructs were treated with erastin (10 μM) for 12 h. Lipid peroxide formation was determined by an MDA assay (g), intracellular glutathione was detected (h), intracellular Fe^{2+} was determined by an iron assay (i), and lipid ROS accumulation was analyzed by flow cytometry (j). Data shown represent mean ± SD from three independent experiments. *$p < 0.05$; **$p < 0.01$; ***$p < 0.001$; ****$p < 0.0001$. MDA, Malondialdehyde; ns, not significant; ROS, reactive oxygen species.

accumulation of MDA, Fe^{2+}, and ROS, and inhibited the production of GSH (Figure 2g-j). However, TXNDC12 overexpression led to the opposite results (Figure S4B–D). These results suggest that the TXNDC12 KD promoted erastin-induced ferroptosis in glioma cells.

TXNDC12 regulates ferroptosis by modulating SLC7A11 expression

To investigate the mechanism of action of TXNDC12 in ferroptosis, TXNDC12 was knocked down and

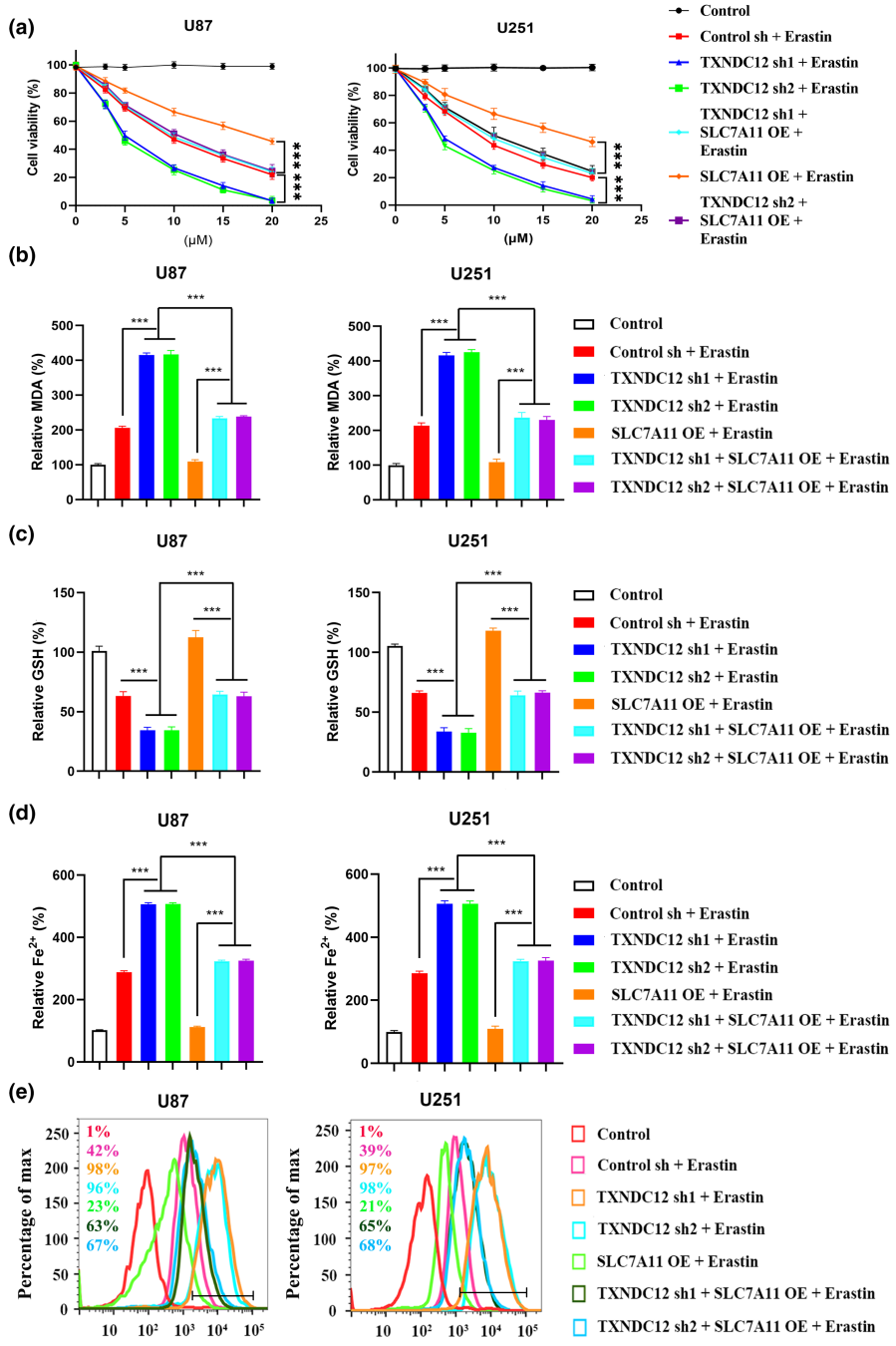

FIGURE 3 TXNDC12 knockdown promotes ferroptosis by regulating SLC7A11. U87 and U251 cells transfected with the indicated constructs were treated with erastin (0–20 μM) for 12 h. Cell viability was determined using a CCK-8 kit (a), lipid peroxide formation was determined by an MDA assay (b), intracellular glutathione was detected (c), the intracellular Fe^{2+} content was determined by an iron assay (d), and lipid ROS accumulation was determined by flow cytometry (e). MDA, malondialdehyde; ROS, reactive oxygen species. ***$p < 0.001$.

differentially expressed genes were characterized to identify the target genes. TXNDC12 KD was transfected, and mRNA levels of ferroptosis-related genes were detected by qPCR (Figure S5A). SLC7A11 was the most downregulated gene. We verified the interaction between TXNDC12 and SLC7A11 by co-immunoprecipitation. Overexpression of SLC7A11 rescued erastin-induced ferroptosis promoted by TXNDC12 KD. Overexpression of SLC7A11 consistently reduced MDA, lipid ROS, and Fe^{2+} levels, and increased the cell viability and GSH levels of TXNDC12 KD cells (Figure 3a-e). TXNDC12 promoted erastin-induced ferroptosis by modulating SLC7A11 expression. At the protein level, when TXNDC12 was knocked down, SLC7A11 protein levels decreased, whereas when TXNDC12 was overexpressed, SLC7A11 protein levels increased (Figure 4a,b). SLC7A11 KD inhibited the expression of several ferroptosis-related proteins promoted by TXNDC12 (Figure 4d). Erastin inhibited SLC7A11 expression; however, TXNDC12 rescued the erastin-induced SLC7A11 protein reduction (Figure 4c-f). TXNDC12 upregulated SLC7A11 expression and inhibited erastin-induced ferroptosis. TXNDC12 alleviates the erastin-induced reduction in SLC7A11 expression.

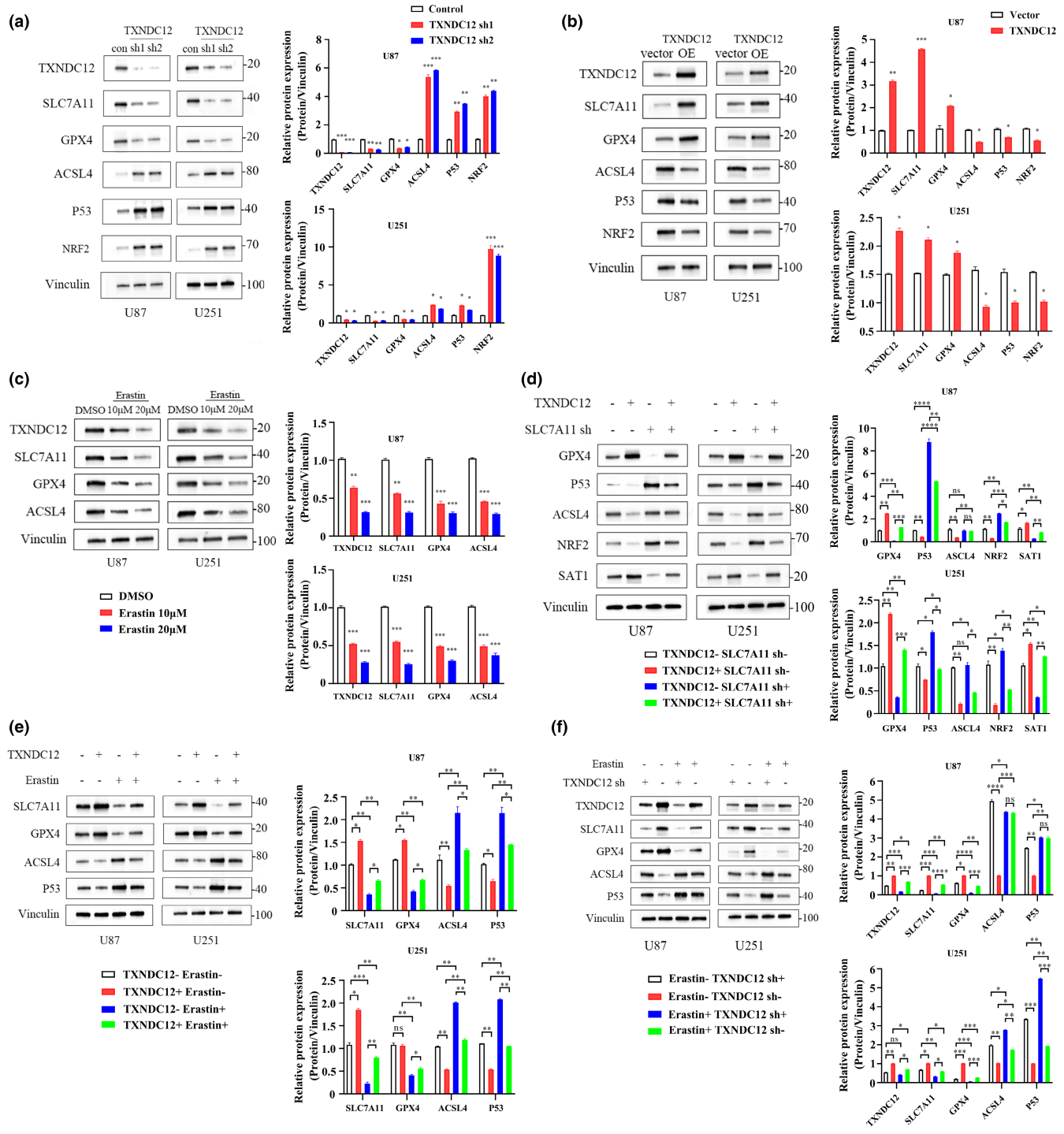

FIGURE 4 TXNDC12 interacts with SLC7A11 in glioma cells. (a) U87 and U251 cells were transfected with control shRNA or TXNDC12 shRNA, and the expression of the indicated proteins was detected by Western blotting. (b) U87 and U251 cells were transfected with an empty vector and TXNDC12 OE, and the expression of the indicated proteins was detected by Western blotting. (c) U87 and U251 cells were treated with DMSO or erastin (10 μM or 20 μM) for 10 h, and the expression of the indicated proteins was detected by Western blotting. (d) U87 and U251 cells were transfected with TXNDC12 OE or SLC7A11 shRNA, and the expression of indicated proteins was detected by Western blotting. (e) U87 and U251 cells transfected with an empty vector and TXNDC12 OE and treated with DMSO or erastin (10 μM), and the expression of the indicated proteins was detected by Western blotting. (f) U87 and U251 cells transfected with control shRNA and TXNDC12 shRNA and treated with DMSO or erastin (10 μM), and the expression of the indicated proteins was detected by Western blotting. Data shown represent mean ± SD from three independent experiments. *$p < 0.05$; **$p < 0.01$; ***$p < 0.001$; ****$p < 0.0001$. DMSO, dimethylsulfoxide; ns, not significant.

TXNDC12 regulates SLC7A11 by directly interacting with SLC7A11

Silver staining was performed on the purified protein complex of the Flag-TXNDC12 U251 stable cell line and parent U251 cell line after lysis (Figure 5a). The 37 kD protein band was analyzed by mass spectrometry, and the peptide sequence was found to match SLC7A11. To clarify the interaction between TXNDC12 and SLC7A11 in vivo, a TXNDC12 expression vector was transfected into U251 cells in the presence or absence of Flag-SLC7A11, and TXNDC12 was detected in the immunoprecipitated Flag-SLC7A11 complex (Figure 5b). SLC7A11 expression vector was transfected into U251 cells in the presence or absence

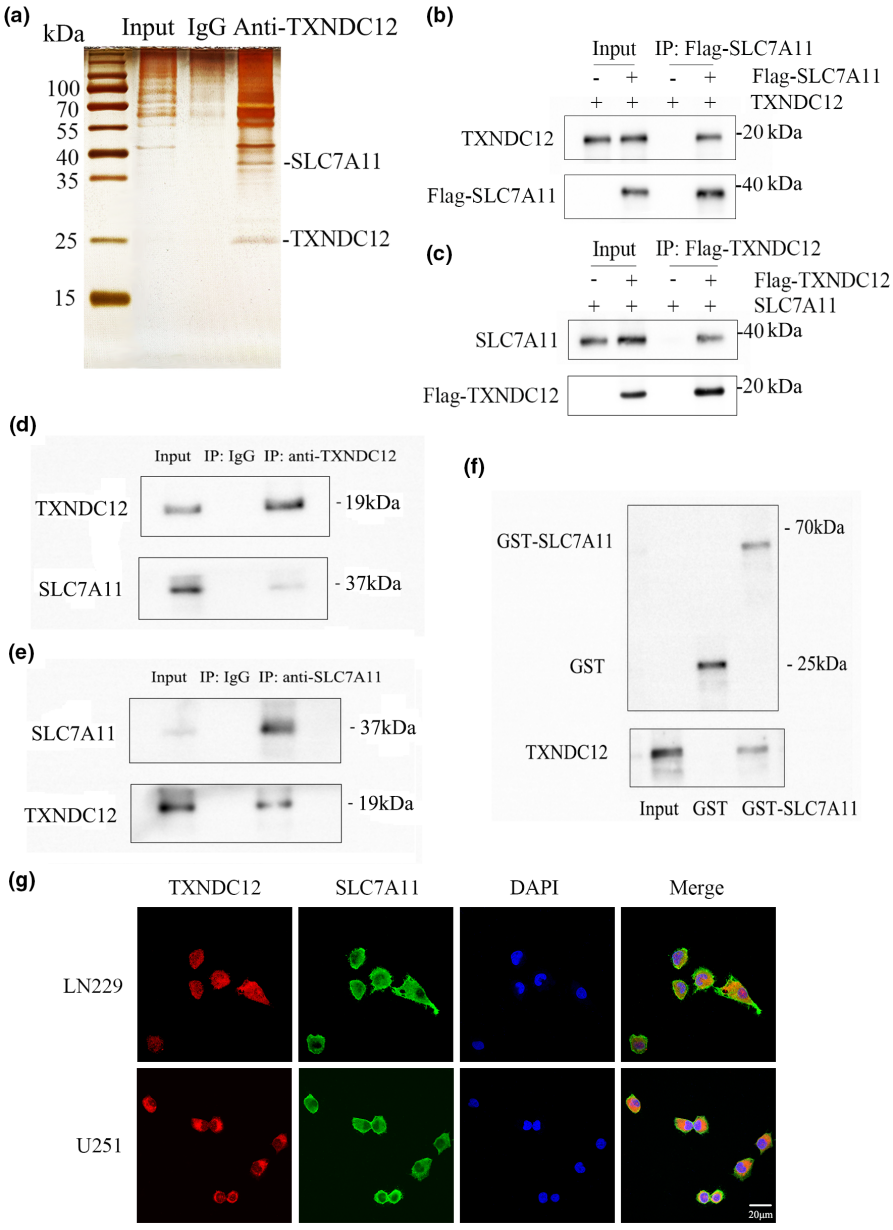

FIGURE 5 TXNDC12 regulates SLC7A11 by directly interacting with SLC7A11. (a) Silver staining of affinity protein purification complexes of the Flag-TXNDC12 U251 stable cell line and parent U251 cell line. (b) The TXNDC12 expression vector was transfected into U251 cells in the presence or absence of Flag-SLC7A11, and TXNDC12 was detected in the immunoprecipitation complex of Flag-SLC7A11. (c) SLC7A11 expression vector was transfected into U251 cells in the presence or absence of Flag-TXNDC12, and SLC7A11 was detected in the immunoprecipitation complex of Flag-TXNDC12. (d) After co-immunoprecipitation of endogenous TXNDC12 from U251 cells, endogenous SLC7A11 was analyzed by Western blotting. (e) After co-immunoprecipitation of endogenous SLC7A11 from U251 cells, endogenous TXNDC12 was analyzed by Western blotting. (f) Interaction between TXNDC12 and SLC7A11, as detected by a GST-pull down experiment. (g) TXNDC12 and SLC7A11 expression in U251 and LN229 cells, as detected by an immunofluorescence assay. The merged images show the overlays of TXNDC12 (red) and SLC7A11 (green). The nuclei were stained with DAPI (blue). Scale bar: 20 μm.

of Flag-TXNDC12, and SLC7A11 was detected in the immunoprecipitated Flag-TXNDC12 complex (Figure 5c). The endogenous protein of U87 cells was used for co-immunoprecipitation, the endogenous TXNDC12 protein was co-precipitated with SLC7A11 specific antibody, and the endogenous SLC7A11 protein was co-precipitated with TXNDC12 specific antibody (Figure 5d,e). Furthermore, the dual immunofluorescence method revealed that TXNDC12 and SLC7A11 were co-localized in the cytoplasm of U251, U87, and LN229 cells (Figure 5g and Figure S5B). To determine whether TXNDC12 and SLC7A11 interact directly, we conducted a GST pull-down experiment and incubated GST-SLC7A11 with TXNDC12, which showed that TXNDC12 could bind to GST-SLC7A11 (Figure 5f). In conclusion, TXNDC12 and SLC7A11 bound to each other both in vivo and in vitro (Figure 6).

TXNDC12 knockdown enhanced the tumor inhibitory effects of erastin in vivo and in vitro

Erastin inhibits the viability of U87 and U251 cells. To determine the effect of TXNDC12 on glioma cells, TXNDC12 KD or TXNDC12 overexpressed lentiviral vectors were stably expressed in U87 and U251 cells, respectively. Erastin was added to the cells. A colony formation assay was performed to determine the effect of TXNDC12 on cell viability. Compared with the control group, cell viability in the erastin and TXNDC12 sh groups decreased. Cell viability was significantly reduced in the TXNDC12 sh + erastin group compared with that in the erastin group. Furthermore, compared to the vector group, cell viability in the vector + erastin group was decreased. Cell viability increased in the TXNDC12 OE + erastin group compared with that in the vector + erastin group. These results indicated that TXNDC12 KD enhanced the erastin-induced cell viability reduction (Figure 2e), and overexpression of TXNDC12 inhibited the erastin-induced cell viability reduction (Figure S4A). At the same time as the lentiviral vectors were being used to stimulate the overexpression of SLC7A11 and TXNDC12 KD in U87 and U251 cells, erastin was added to treat the cells, and the effect of TXNDC12 on cell viability was determined by a colony formation assay. Compared to the TXNDC12 sh + erastin group, the cell viability of the TXNDC12 sh + SLC7A11 OE + erastin group was significantly improved. The decrease in cell viability induced by TXNDC12 KD was rescued by SLC7A11 (Figure 7a). We investigated the effect of TXNDC12 on the antitumor activity of erastin in vivo. U87 cells stably expressing TXNDC12 KD or SLC7A11 were injected intracranially into BALB/c female immunodeficient nude mice and treated with erastin for 7 days. These results indicated that TXNDC12 KD enhanced erastin-induced tumor inhibition, which was rescued by SLC7A11 (Figure 7b-f). In conclusion, TXNDC12 KD enhanced erastin-induced tumor inhibition in vivo and in vitro.

DISCUSSION

In this study, we found that high TXNDC12 levels were associated with a higher glioma grade, poor prognosis, and low survival rates. TXNDC12 KD promoted an erastin-induced decrease in glioma cell viability TXNDC12 KD significantly promoted the

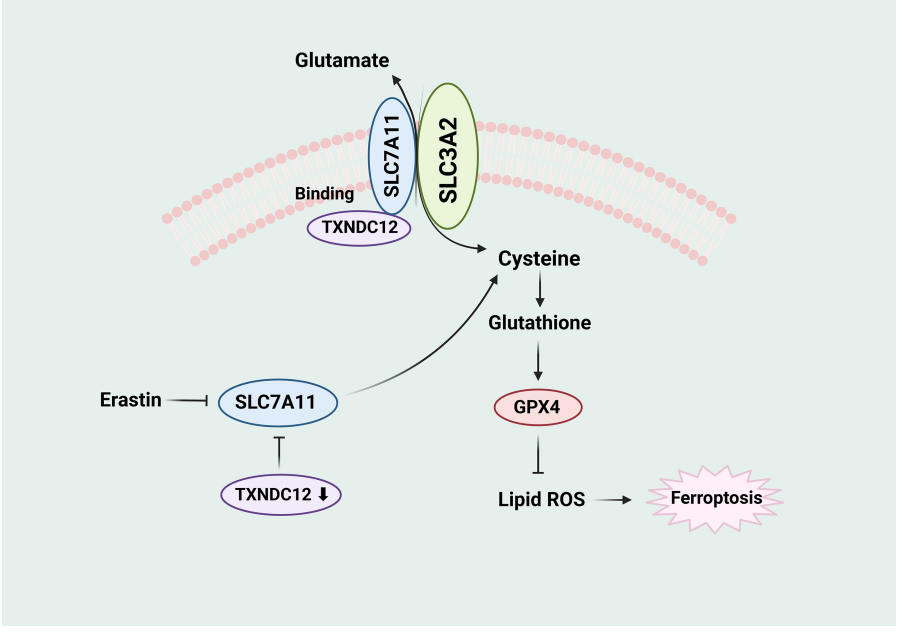

FIGURE 6 Schematic model of TXNDC12 in regulating ferroptosis in glioma cells.

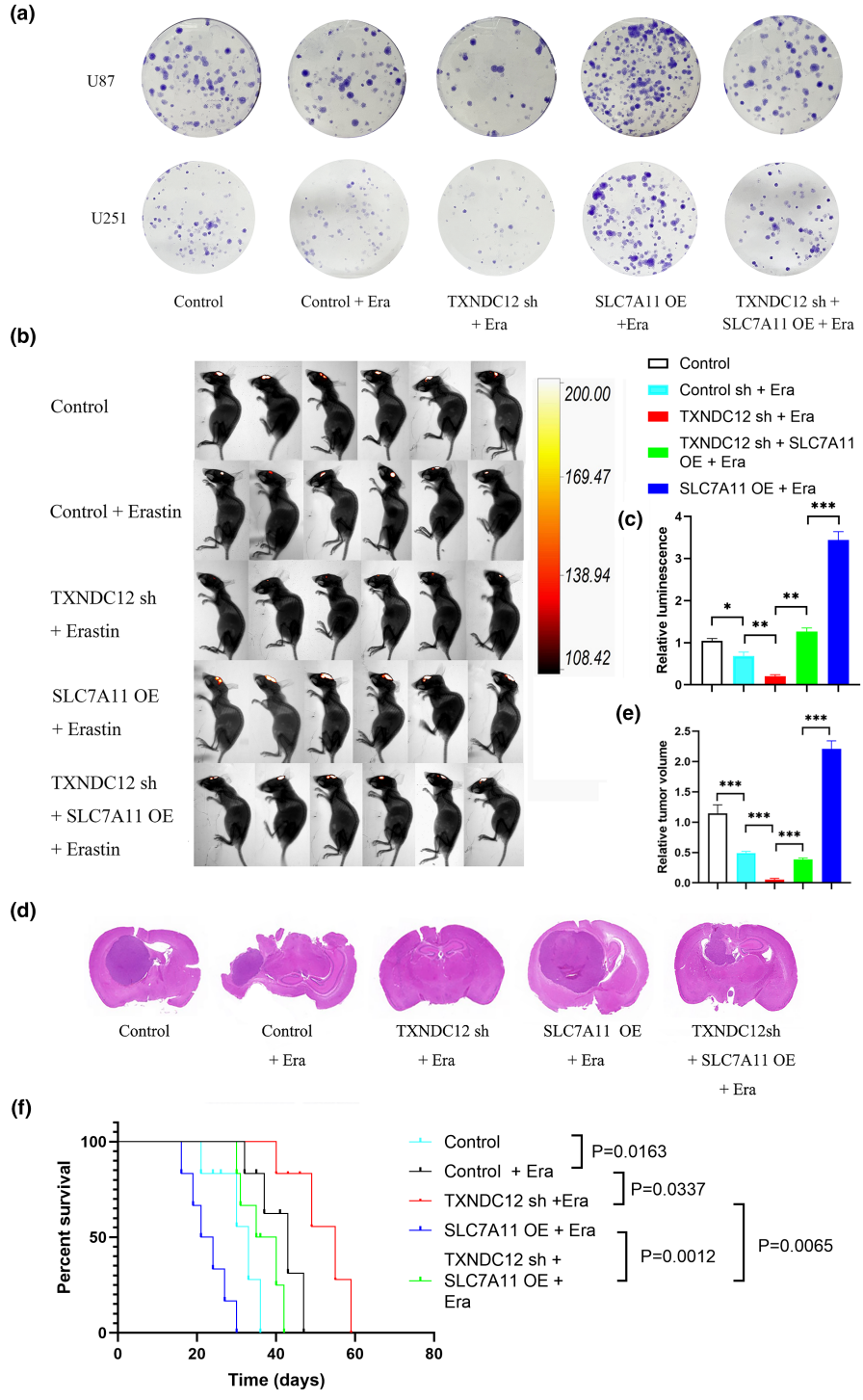

FIGURE 7 TXNDC12 knockdown can enhance tumor inhibitory effects of erastin. (a) Representative images of clonability analysis of U87 and U251 cells transfected with control, TXNDC12 shRNA, or SLC7A11 and treated with DMSO or erastin (10 μM). (b,c) Control, TXNDC12 shRNA, or SLC7A11 U87 cells were transplanted into the craniums of immunodeficient 5-week-old nude mice (5×10^5 cells/mouse). Starting on day 7, erastin (15 mg/kg intracranial injection twice every other day) was administered to treat the tumors in situ. Tumor formation was assessed using bioluminescence imaging on day 20. (d) Representative images of H&E staining of intracranial tumor sections from mice. (e) Relative volume of H&E-stained sections of intracranial tumors in mice. (f) Kaplan–Meier animal survival analysis ($n = 6$ mice/group). Data shown represent mean ± SD from three independent experiments. Comparisons were made using the Student's *t*-test. ***$p < 0.001$. H&E, hematoxylin and eosin; ns, not significant; ROS, reactive oxygen species.

erastin-induced accumulation of MDA, Fe^{2+}, and ROS levels, and inhibited the production of GSH. Through co-immunoprecipitation and GST pull-down assays, TXNDC12 was found to interact with SLC7A11. SLC7A11 is regulated by TXNDC12, and TXNDC12 KD decreases SLC7A11 protein levels. Erastin inhibited SLC7A11 expression and TXNDC12 alleviated erastin-induced SLC7A11 expression reduction. Overexpression of SLC7A11 rescued erastin-induced ferroptosis promoted by TXNDC12 KD. In addition, TXNDC12 KD promoted erastin-induced glioma cell inhibition, which was rescued by SLC7A11 treatment.

Gliomas are the most common primary intracranial tumors.[23] Glioma is a malignant tumor with little tendency for distant metastasis, and its prognosis depends almost entirely on tumor grade rather than stage.[24,25] According to the WHO classification criteria, gliomas are classified into grades I, II, III, and IV according to the malignancy of the tumor.[26] A higher grade indicates a higher malignancy, followed by a worse prognosis.[27] The current

treatment for grade I glioma is curable, and the survival time for grade II gliomas is usually greater than 10 years.[28] The survival time of patients with grade III glioma can be up to 3 years, and long-term survival can be achieved with good treatment effects.[29] The average survival time for patients with grade IV gliomas is greater than a year, and few patients can survive for greater than 5 years.[30,31] Gliomas are typically treated with surgical resection, radiotherapy, and chemotherapy, although it is difficult to improve the OS rate of patients.[32,33] Recently, tumor treating fields therapy has emerged as a new local antitumor treatment mode using low-intensity and medium frequency electrical fields.[34] Glioma treatment can be moderately improved using this approach.[35] However, the OS of patients with glioma did not significantly improve due to the rapid proliferation, strong invasion, and treatment resistance of gliomas.[36]

Ferroptosis has been linked to cancer, and many cancer-related genes are involved in its regulation. Tumor cells rely on their strong antioxidant capacity to escape ferroptosis.[37] Therefore, studying ferroptosis may be an important research direction for interfering with tumor proliferation and invasion.[38] Similar to most tumors, gliomas are closely associated with ferroptosis.[39] Glioma cells are strongly dependent on iron. Iron chelates induce apoptosis and exhibit antitumor effects in cancer therapy.[40] In glioma tissues, the expression of GPX4 and SLC7A11, the key regulatory factors of ferroptosis, is increased, which may be related to the poor prognosis of glioma.[41] System Xc^- is an important factor that regulates the proliferation of gliomas, and glutamic acid released by glioma cells can promote glioma growth. However, studies on ferroptosis in gliomas are still at a developing stage.[42]

The protein disulfide isomerase (PDI) family member TXNDC12 plays a vital role in cancer progression and occurrence. PDI is involved in disulfide bond formation during protein folding.[43] Members of the PDI family can regulate the proliferation, invasion, and metastasis of brain, lymphoma, kidney, ovarian, prostate, and lung cancers. Several studies have reported that PDI can be used as a therapeutic target in cancer.[44] TXNDC12 overexpression stimulates nuclear translocation and β-catenin activation, thereby enabling the ZEB1-mediated EMT to promote hepatocellular carcinoma metastasis.[15] Tumor size, lymph node metastasis, and poor clinical outcomes are correlated with TXNDC12 expression in gastric cancer. Moreover, by inhibiting gastric cancer growth and migration/invasion, as well as downregulating the phosphorylation of FAK and paxlin, TXNDC12 knockout has the potential to affect carcinogenesis and metastasis of gastric cancer by activating the FAK signaling pathway.[17] However, the specific role of TXNDC12 in gliomas remains unclear. It can, however, be concluded that TXNDC12 contributes to a poor prognosis in gliomas. We found a significant correlation between TXNDC12 expression and the expression of some ferroptosis-related genes, such as GPX4, ALOX5AP, and SLC7A11.[45]

Targeted therapy has made great progress in cancer treatment, and the use of specific drugs targeting tumor biomarkers can improve patient survival rate.[46] Erlotinib can be used for patients with lung cancer harboring *EGFR* mutations.[47] Patients with *HER2* mutations can be treated with trastuzumab to control the spread of breast cancer.[48] Our results indicate that TXNDC12 KD promoted erastin-induced glioma cell inhibition. Therefore, we propose combining a TXNDC12 inhibitor with the iron death inducer erastin to promote iron death in glioma cells, thereby inhibiting glioma growth and progression.

One limitation of our study was that we did not use an inhibitor of TXNDC12. We have not produced TXNDC12 inhibitors and have not acquired any clinical development of TXNDC12 inhibitors. TXNDC12 inhibitors are the key to evaluating whether TXNDC12 can be used to treat glioma with ferroptosis. Many factors need to be considered when using TXNDC12 inhibitors in glioma treatment, such as whether TXNDC12 inhibitors can penetrate the BBB, the length of their half-life, and their side effects. These factors will shape the direction of future research.

In summary, we investigated the function of TXNDC12 in gliomas and ferroptosis. TXNDC12 plays a vital role in ferroptosis by modulating SLC7A11 expression, and downregulation of TXNDC12 promoted an erastin-induced reduction in glioma cell activity. This suggests that TXNDC12 is involved in ferroptosis, which may be a direction for future studies on ferroptosis in gliomas and for the treatment of gliomas.

AUTHOR CONTRIBUTIONS

H.Y. and K.Z. wrote the manuscript. X.J. designed the research. H.Y. and K.Z. performed the research. M.W. analyzed the data. H.Y. and M.W. contributed new reagents/analytical tools.

ACKNOWLEDGMENTS

The authors thank all the people who helped us with this study.

FUNDING INFORMATION

This research was supported by the National Natural Science Foundation of China (grant number: 82203140).

CONFLICT OF INTEREST STATEMENT

The authors declared no competing interests for this work.

DATA AVAILABILITY STATEMENT

The dataset involved or analyzed during the study can be obtained from the corresponding author upon reasonable request.

ETHICS STATEMENT

This study was conducted in accordance with the guidelines of the Declaration of Helsinki and approved by the Ethics Committee of the Tongi Medical College, Huazhong University of Science and Technology (protocol code: [2019] IEC (S742). Date of approval: March 4, 2019).

ORCID

Xiaobing Jiang https://orcid.org/0000-0002-0262-1164

REFERENCES

1. Wang DD, Deng H, Hervey-Jumper SL, Molinaro AA, Chang EF, Berger MS. Seizure outcome after surgical resection of insular glioma. *Neurosurgery*. 2018;83(4):709-718.
2. Verburg N, Barthel FP, Anderson KJ, et al. Spatial concordance of DNA methylation classification in diffuse glioma. *Neuro Oncol*. 2021;23(12):2054-2065.
3. Lah TT, Novak M, Breznik B. Brain malignancies: glioblastoma and brain metastases. *Semin Cancer Biol*. 2020;60:262-273.
4. Mellinghoff IK, Ellingson BM, Touat M, et al. Ivosidenib in isocitrate dehydrogenase 1-mutated advanced glioma. *J Clin Oncol*. 2020;38(29):3398-3406.
5. Tomar MS, Kumar A, Srivastava C, Shrivastava A. Elucidating the mechanisms of temozolomide resistance in gliomas and the strategies to overcome the resistance. *Biochim Biophys Acta Rev Cancer*. 2021;1876(2):188616.
6. Carpenter AB, Carpenter AM, Aiken R, Hanft S. Oncolytic virus in gliomas: a review of human clinical investigations. *Ann Oncol*. 2021;32(8):968-982.
7. Mou Y, Wang J, Wu J, et al. Ferroptosis, a new form of cell death: opportunities and challenges in cancer. *J Hematol Oncol*. 2019;12(1):34.
8. Liang D, Minikes AM, Jiang X. Ferroptosis at the intersection of lipid metabolism and cellular signaling. *Mol Cell*. 2022;82(12):2215-2227.
9. Chen X, Yu C, Kang R, Kroemer G, Tang D. Cellular degradation systems in ferroptosis. *Cell Death Differ*. 2021;28(4):1135-1148.
10. Parker JL, Deme JC, Kolokouris D, et al. Molecular basis for redox control by the human cystine/glutamate antiporter system xc(). *Nat Commun*. 2021;12(1):7147.
11. Hassannia B, Vandenabeele P, Vanden Berghe T. Targeting ferroptosis to iron out cancer. *Cancer Cell*. 2019;35(6):830-849.
12. Ursini F, Maiorino M. Lipid peroxidation and ferroptosis: the role of GSH and GPx4. *Free Radic Biol Med*. 2020;152:175-185.
13. Zhang C, Liu X, Jin S, Chen Y, Guo R. Ferroptosis in cancer therapy: a novel approach to reversing drug resistance. *Mol Cancer*. 2022;21(1):47.
14. Jeong W, Lee DY, Park S, Rhee SG. ERp16, an endoplasmic reticulum-resident thiol-disulfide oxidoreductase: biochemical properties and role in apoptosis induced by endoplasmic reticulum stress. *J Biol Chem*. 2008;283(37):25557-25566.
15. Yuan K, Xie K, Lan T, et al. TXNDC12 promotes EMT and metastasis of hepatocellular carcinoma cells via activation of β-catenin. *Cell Death Differ*. 2020;27(4):1355-1368.
16. Kang J, Xiang X, Chen X, et al. Angiogenesis-related gene signatures reveal the prognosis of cervical cancer based on single cell sequencing and co-expression network analysis. *Front Cell Dev Biol*. 2022;10:1086835.
17. Wu J, Chen XH, Wang XQ, et al. ERp19 contributes to tumorigenicity in human gastric cancer by promoting cell growth, migration and invasion. *Oncotarget*. 2015;6(14):11794-11805.
18. Galvan A, Frullanti E, Anderlini M, et al. Gene expression signature of non-involved lung tissue associated with survival in lung adenocarcinoma patients. *Carcinogenesis*. 2013;34(12):2767-2773.
19. Wang X, Yang Q, Liu N, Bian Q, Gao M, Hou X. Clinical value of TXNDC12 combined with IDH and 1p19q as biomarkers for prognosis of glioma. *Pathol Oncol Res*. 2021;27:1609825.
20. Jia D, Li S, Li D, Xue H, Yang D, Liu Y. Mining TCGA database for genes of prognostic value in glioblastoma microenvironment. *Aging (Albany NY)*. 2018;10(4):592-605.
21. Goldsmith JD, Fitzgibbons PL, Swanson PE. Principles of analytic validation of clinical immunohistochemistry assays. *Adv Anat Pathol*. 2015;22(6):384-387.
22. Taylor SC, Rosselli-Murai LK, Crobeddu B, Plante I. A critical path to producing high quality, reproducible data from quantitative western blot experiments. *Sci Rep*. 2022;12(1):17599.
23. Lapointe S, Perry A, Butowski NA. Primary brain tumours in adults. *Lancet*. 2018;392(10145):432-446.
24. Yadav G, Kulshreshtha R. Metastasis associated long noncoding RNAs in glioblastoma: biomarkers and therapeutic targets. *J Cell Physiol*. 2022;237(1):401-420.
25. Weller M, Wick W, Aldape K, et al. Glioma. *Nat Rev Dis Primers*. 2015;1:15017.
26. Perez A, Huse JT. The evolving classification of diffuse gliomas: World Health Organization updates for 2021. *Curr Neurol Neurosci Rep*. 2021;21(12):67.
27. Zhou Q, Xue C, Ke X, Zhou J. Treatment response and prognosis evaluation in high-grade glioma: an imaging review based on MRI. *J Magn Reson Imaging*. 2022;56(2):325-340.
28. Dworkin M, Mehan W, Niemierko A, et al. Increase of pseudoprogression and other treatment related effects in low-grade glioma patients treated with proton radiation and temozolomide. *J Neurooncol*. 2019;142(1):69-77.
29. Bunevicius A, Pikis S, Padilla F, Prada F, Sheehan J. Sonodynamic therapy for gliomas. *J Neurooncol*. 2022;156(1):1-10.
30. Omuro A, Deangelis LM. Glioblastoma and other malignant gliomas: a clinical review. *Jama*. 2013;310(17):1842-1850.
31. Poff A, Koutnik AP, Egan KM, Sahebjam S, D'Agostino D, Kumar NB. Targeting the Warburg effect for cancer treatment: ketogenic diets for management of glioma. *Semin Cancer Biol*. 2019;56:135-148.
32. Mcbain C, Lawrie TA, Rogozińska E, et al. Treatment options for progression or recurrence of glioblastoma: a network meta-analysis. *Cochrane Database Syst Rev*. 2021;5(1):Cd013579.
33. Choi S, Yu Y, Grimmer MR, Wahl M, Chang SM, Costello JF. Temozolomide-associated hypermutation in gliomas. *Neuro Oncol*. 2018;20(10):1300-1309.
34. Wenger C, Miranda PC, Salvador R, et al. A review on tumor-treating fields (TTFields): clinical implications

inferred from computational modeling. *IEEE Rev Biomed Eng*. 2018;11:195-207.
35. Ghiaseddin AP, Shin D, Melnick K, Tran DD. Tumor treating fields in the Management of Patients with malignant gliomas. *Curr Treat Options Oncol*. 2020;21(9):76.
36. Yang P, Wang Y, Peng X, et al. Management and survival rates in patients with glioma in China (2004-2010): a retrospective study from a single-institution. *J Neurooncol*. 2013;113(2):259-266.
37. Zhao L, Zhou X, Xie F, et al. Ferroptosis in cancer and cancer immunotherapy. *Cancer Commun (Lond)*. 2022;42(2):88-116.
38. Li D, Li Y. The interaction between ferroptosis and lipid metabolism in cancer. *Signal Transduct Target Ther*. 2020;5(1):108.
39. Zhan S, Lu L, Pan SS, et al. Targeting NQO1/GPX4-mediated ferroptosis by plumbagin suppresses in vitro and in vivo glioma growth. *Br J Cancer*. 2022;127(2):364-376.
40. Lu S, Wang XZ, He C, et al. ATF3 contributes to brucine-triggered glioma cell ferroptosis via promotion of hydrogen peroxide and iron. *Acta Pharmacol Sin*. 2021;42(10):1690-1702.
41. Li S, He Y, Chen K, et al. RSL3 drives ferroptosis through NF-κB pathway activation and GPX4 depletion in glioblastoma. *Oxid Med Cell Longev*. 2021;2021:2915019.
42. De Souza I, Monteiro LKS, Guedes CB, et al. High levels of NRF2 sensitize temozolomide-resistant glioblastoma cells to ferroptosis via ABCC1/MRP1 upregulation. *Cell Death Dis*. 2022;13(7):591.
43. Rowe ML, Ruddock LW, Kelly G, Schmidt J̈M, Williamson RA, Howard MJ. Solution structure and dynamics of ERp18, a small endoplasmic reticulum resident oxidoreductase. *Biochemistry*. 2009;48(21):4596-4606.
44. Powell LE, Foster PA. Protein disulphide isomerase inhibition as a potential cancer therapeutic strategy. *Cancer Med*. 2021;10(8):2812-2825.
45. Zhang W, Yao S, Huang H, et al. Molecular subtypes based on ferroptosis-related genes and tumor microenvironment infiltration characterization in lung adenocarcinoma. *Onco Targets Ther*. 2021;10(1):1959977.
46. Zhou Z, Li M. Targeted therapies for cancer. *BMC Med*. 2022;20(1):90.
47. Cao Q, You X, Xu L, Wang L, Chen Y. PAQR3 suppresses the growth of non-small cell lung cancer cells via modulation of EGFR-mediated autophagy. *Autophagy*. 2020;16(7):1236-1247.
48. Von Minckwitz G, Huang CS, Mano MS, et al. Trastuzumab Emtansine for residual invasive HER2-positive breast cancer. *N Engl J Med*. 2019;380(7):617-628.

SUPPORTING INFORMATION

Additional supporting information can be found online in the Supporting Information section at the end of this article.

How to cite this article: Yu H, Zhu K, Wang M, Jiang X. TXNDC12 knockdown promotes ferroptosis by modulating SLC7A11 expression in glioma. *Clin Transl Sci*. 2023;16:1957-1971. doi:10.1111/cts.13604